Hydrol. Earth Syst. Sci. Discuss., 10, 13783–13816, 2013
www.hydrol-earth-syst-sci-discuss.net/10/13783/2013/
doi:10.5194/hessd-10-13783-2013

Hydrology and Earth System Sciences
Open Access
Discussions

The suitability of remotely sensed soil moisture for improving operational flood forecasting

N. Wanders[1], **D. Karssenberg**[1], **A. de Roo**[1,2], **S. M. de Jong**[1], **and M. F. P. Bierkens**[1,3]

[1]Department of Physical Geography, Utrecht University, Utrecht, the Netherlands
[2]European Commission, Join Research Centre, Ispra, Italy
[3]Deltares, Utrecht, the Netherlands

Received: 1 November 2013 – Accepted: 6 November 2013 – Published: 14 November 2013

Correspondence to: N. Wanders (n.wanders@uu.nl)

Published by Copernicus Publications on behalf of the European Geosciences Union.

Abstract

We evaluate the added value of assimilated remotely sensed soil moisture for the European Flood Awareness System (EFAS) and its potential to improve the prediction of the timing and height of the flood peak and low flows. EFAS is an operational flood forecasting system for Europe and uses a distributed hydrological model for flood predictions with lead times up to 10 days. For this study, satellite-derived soil moisture from ASCAT, AMSR-E and SMOS is assimilated into the EFAS system for the Upper Danube basin and results are compared to assimilation of discharge observations only. To assimilate soil moisture and discharge data into EFAS, an Ensemble Kalman Filter (EnKF) is used. Information on the spatial (cross-) correlation of the errors in the satellite products, is included to ensure optimal performance of the EnKF. For the validation, additional discharge observations not used in the EnKF, are used as an independent validation dataset.

Our results show that the accuracy of flood forecasts is increased when more discharge observations are assimilated; the Mean Absolute Error (MAE) of the ensemble mean is reduced by 65 %. The additional inclusion of satellite data results in a further increase of the performance: forecasts of base flows are better and the uncertainty in the overall discharge is reduced, shown by a 10 % reduction in the MAE. In addition, floods are predicted with a higher accuracy and the Continuous Ranked Probability Score (CRPS) shows a performance increase of 5–10 % on average, compared to assimilation of discharge only. When soil moisture data is used, the timing errors in the flood predictions are decreased especially for shorter lead times and imminent floods can be forecasted with more skill. The number of false flood alerts is reduced when more data is assimilated into the system and the best performance is achieved with the assimilation of both discharge and satellite observations.

The additional gain is highest when discharge observations from both upstream and downstream areas are used in combination with the soil moisture data. These results

HESSD

10, 13783–13816, 2013

show the potential of remotely sensed soil moisture observations to improve near-real time flood forecasting in large catchments.

1 Introduction

Floods are extreme hydrological events caused by excessive water availability and may cause large economical, societal and natural damage. One example is the summer 2013 flood in central Europe producing historical high water levels in large parts of the Danube and Elbe catchments, causing a total estimated economic loss of 23 billion Euro (Claims Journal, 2013). Due to their increasing impact on society, forecasting of these extreme events has become more important to increase preparedness and improve the response to and prevention of floods. This requires an increasing need to develop accurate and reliable flood forecasting systems. For transboundary river basins, national forecasting systems are often not sufficient and transboundary forecasting systems are required. To fulfil this need, the European Commission developed the European Flood Awareness System (EFAS) for flood forecasting up to a leadtime of 10 days for the European continent (Thielen et al., 2009). Flood forecasts are made for multiple basins, using distributed hydrological modelling. Systems like EFAS are highly dependent on the meteorological forcing provided as well as the pre-storm initial conditions of the catchment (Nester et al., 2012; Alfieri et al., 2013).

To improve estimates of initial conditions data assimilation techniques have the potential to correct incorrect model states with observational data to obtain the best possible estimate of the current status of the hydrological system. Discharge data is often used in these data assimilation frameworks, because it contains the integrated information of all other hydrological states (e.g. Vrugt et al., 2006; Clark et al., 2008; Rakovec et al., 2012). For example, Bogner and Pappenberger (2011) applied a posteriori wavelet based error correction method on the EFAS forecasts, which is now also used in the operational EFAS. However, it is difficult to obtain these measurements in real-time in a way they can be used in EFAS. Measurements of hydrological

HESSD
10, 13783–13816, 2013

states other than discharge are rarely used for estimating the model's initial state while these may be of considerable value. In particular, measurements of the pre-storm soil moisture conditions could potentially improve flood forecasting systems, since initial soil moisture conditions are expected to have a large impact on the flood peaks during a storm event. The soil moisture content determines the amount of water which can still be stored in the unsaturated zone or percolate to the saturated zone and thereby influences the precipitation required to generate overland flow. However, field observations at continental scale are not available due to the limited number of observational networks and their low spatial support. Remotely sensed soil moisture retrievals from the microwave domain could potentially fill the need for soil moisture observations at the large spatial scales. Observations are globally available and revisit times per sensor are between 1 and 3 days depending on latitude.

Multiple studies have used remotely sensed soil moisture to improve discharge simulations in small catchments ($\leq 1000\,km^2$) and to correct for errors in pre-storm soil moisture conditions (Pauwels et al., 2001; Scipal et al., 2008; Bolten et al., 2010; Brocca et al., 2010; Liu et al., 2011; Brocca et al., 2012). These studies show that assimilation of these data improved the simulation of flood events and especially the height of the flood peak. For large-scale catchments, Draper et al. (2011) assimilated remotely sensed soil moisture from ASCAT over France to improve discharge simulations. It was concluded that the assimilation of soil moisture mainly corrected for biases in precipitation or incorrect model climatology. The potential to improve flood forecasts was not studied. The previously mentioned studies mainly study the potential gain for flood forecasting, when only observations from a single sensor are assimilated. This potential can be increased by making use of soil moisture retrieved by multiple sensors, thereby increasing the quality and quantity of the observations. The value of combined assimilation of data from multiple sensors for operational flood forecasting at large-scale remains however unknown. Additionally the added value of the remotely sensed soil moisture compared to the assimilation of discharge observations has not been extensively explored. Therefore, more research is required, especially in large-scale

HESSD
10, 13783–13816, 2013

catchments using conjunctively multi-sensor remotely sensed soil moisture observations and discharge data.

The aim of this study is to determine the benefits of the assimilation of multi-sensor soil moisture observations in operational flood forecasting systems in large scale catchments. To achieve this aim, this research focuses on two main research questions: (i) Does the assimilation of remotely sensed soil moisture lead to increased forecasting skills in terms of forecast uncertainty and forecast bias compared to assimilation of discharge observations? (ii) Does the assimilation of remotely sensed soil moisture increase the lead times at which floods can be accurately predicted? (iii) Is it possible to reduce the number of false flood alerts with the use of remotely sensed soil moisture? These research questions are answered using the EFAS model setup, which enables a proper validation of the results in the context of a real operational system. Results of assimilating remotely sensed soil moisture are compared with assimilation of discharge data only. Also, the impact of the number of discharge observations is investigated, to properly validate in what situations the assimilation of remotely sensed soil moisture could improve flood forecasting. As a test-basin the Upper Danube catchment is selected which is one of the largest catchments in Europe containing a large number of locations with timeseries of discharge. Satellite data from three microwave sensors (ASCAT, AMSR-E and SMOS) is used in the assimilation framework to increase the number of observations and the potential benefits of these observations for the flood predictions.

2 Material and methods

2.1 Study area

The study area is the Upper Danube catchment upstream of Bratislava (catchment size 135×10^3 km, Fig. 1). The border of the Upper Danube is formed by the Alps in the South and the catchment contains the northern part of Austria, the southern

HESSD
10, 13783–13816, 2013

part of Germany, the South-eastern part of the Czech Republic and western Slovakia. Elevations range from 150–3150 m a.s.l. In the catchment, daily discharge observations for 23 locations are available through the Global Runoff Data Centre (GRDC) which enable validation and assimilation (Fig. 1).

2.2 European Flood Awareness System

The European Flood Awareness System was developed in 2003 by the European Commission at the Joint Research Centre in Ispra and is being improved since[1]. In 2012 EFAS because an operational service aiming to provide flood forecasts up to 10 days in advance over the European continent. At the core of the EFAS system is the hydrological model LISFLOOD which was originally developed by De Roo et al. (2000), later improved by Van Der Knijff et al. (2010) and running in the PCRaster modelling environment (Wesseling et al., 1996; Karssenberg et al., 2010). LISFLOOD was specifically developed for discharge simulations of large scale river basins. In this study, two additional shallow layers were added to the unsaturated zone to enable a simulation of soil moisture at the typical penetration depth of the microwave sensors, used for retrieving remotely sensed soil moisture. A full description of the modifications is given by Wanders et al. (2013). The model consists of a vegetation layer, four layers to simulate the unsaturated zone, two linear reservoirs to represent fast and slow responding groundwater systems and a channel network for discharge routing (Fig. 2). The meteorological forcing of LISFLOOD consists of daily precipitation, daily potential evapotranspiration and the average daily temperature. EFAS uses meteorological forcing from the 51 members of the European Centre for Medium-Range Weather Forecasting Ensemble Prediction System (ECMWF-EPS). This, results in 51 hydrological forecasts for every 12 h at midday and midnight.

In order to use the best calibrated model for the study area, the probabilistic model calibration set-up from Wanders et al. (2013) was used. The parameters which were

[1] www.efas.eu

HESSD
10, 13783–13816, 2013

calibrated were related to the snow accumulation, infiltration and percolation through the unsaturated zone, the groundwater system and routing of discharge (Fig. 2). This resulted in calibrated parameters with distributions defined by 300 realizations of parameter sets, which could be used for hydrological simulations. The use of this parameter distributions allows to account for the uncertainty in the initial conditions, while the current EFAS uses fixed initial conditions for the hydrological forecast. The new model set-up will allow for a better estimation of the forecast uncertainty, especially when initial conditions influence the hydrological simulations.

2.3 Data

2.3.1 Satellite data

Remotely sensed soil moisture data from three satellites is used, namely SMOS, ASCAT and AMSR-E. SMOS is the first dedicated soil moisture satellite using fully polarized passive microwave signals at 1.41 GHz (L-band) observed at multiple angles (Kerr et al., 2012). The observation depth of SMOS is 5 cm with a spatial resolution of 35–50 km depending on the incident angle and the deviation from the satellite ground track. The revisit time of SMOS is within 3 days depending on the latitude. SMOS retrievals which are potentially contaminated with Radio Frequency Interference (RFI) have been removed.

AMSR-E is a multi-frequency passive microwave radiometer (6.9 GHz, C-band) and is a widely used sensor for soil moisture retrievals. The spatial resolution of AMSR-E is between 36 and 54 km with an observation depth of 2 cm and a revisit time of 3 days. Several algorithms estimating surface soil moisture from AMSR-E observations exist (e.g. Njoku et al., 2003; Owe et al., 2008). One of the algorithms using exclusively satellite observations is the Land Parameter Retrieval Model (LPRM) which was used for this study. LPRM soil moisture products have been validated against in situ observations (e.g. Wagner et al., 2007; De Jeu et al., 2008; Draper et al., 2009), models (e.g.

HESSD
10, 13783–13816, 2013

Loew et al., 2009; Crow et al., 2010; Bisselink et al., 2011) and other satellite products (e.g. Wagner et al., 2007; Dorigo et al., 2010).

Unlike SMOS and AMSR-E, ASCAT uses active microwave at a frequency of 5.3 GHz (C-band) to determine the soil moisture content (Wagner et al., 1999; Naeimi et al., 2009). ASCAT uses a change detection method (Naeimi et al., 2009) and data is provided relative to the soil moisture content of the wettest (field capacity) and driest (wilting point) soil moisture conditions measured (Wagner et al., 1999). The spatial resolution of ASCAT is around 25 km, the observation depth is 2 cm and the temporal resolution equals a revisit time of 3 days.

All satellite soil moisture products are used on an equal area Discrete Global Grid product (DGG). For the SMOS and ASCAT soil moisture product a DGG is available (Bartalis et al., 2006), while for the AMSR-E product a DGG is not available. Therefore, the AMSR-E data was projected on the DGG of SMOS using the nearest neighbour approach, because both satellites have roughly the same spatial resolution. The DGG of ASCAT uses equally spaced areas of 12.5 km while the other DGG uses a slightly lower resolution of 15 km between points.

Although the passive microwave satellite missions, SMOS and AMSR-E, give absolute soil moisture values in $m^3\,m^{-3}$, all satellite data was converted using a rescaling approach. The converted satellite values $\theta_{s,\,new}$ in $m^3\,m^{-3}$ used for calibration are calculated by:

$$\theta_{s,\,new} = \frac{\theta_s - \theta_{s,5}}{\theta_{s,95} - \theta_{s,5}}(\theta_{FC} - \theta_{WP}) + \theta_{WP} \quad (1)$$

where θ_s are the observed satellite soil moisture values (–) at a DGG location, $\theta_{s,95}$ and $\theta_{s,5}$ are the 95th and 5th percentiles of satellite soil moisture values at the DGG location respectively (–), θ_{FC} and θ_{WP} are field capacity and wilting point of the modelled soil moisture values ($m^3\,m^{-3}$) at the DGG location. The average model values, θ_{FC} and θ_{WP}, are dependent on the soil texture and are averaged over the support unit of the satellite retrieval.

HESSD
10, 13783–13816, 2013

Frozen soils, snow accumulation and RFI hamper the soil moisture retrieval due to changes in the dielectric constant when water freezes. Therefore, retrievals done with (1) an air temperature below 4 °C, (2) simulated snow accumulation and (3) the presence of RFI were not used in the calibration.

2.3.2 Discharge data

The Upper Danube catchment contains 23 locations where daily discharge observations are available (Fig. 1). Timeseries of discharge are available from January 2000 until December 2011. Using a split sample approach the discharge of 7 stations was used for data assimilation into the forecasting system, while the other 16 stations were only used for validations of the forecasts. Assimilation and validation stations are selected such that they are equally distributed over the catchment and are situated both in small rivers and the main Upper Danube river. This will allow to evaluate the impact of the data assimilation at different catchment sizes within the Upper Danube catchment.

2.4 Data assimilation

The Ensemble Kalman Filter (EnKF) is a Monte Carlo based approach which is highly suitable for data assimilation in high dimensional systems (Evensen, 1994, 2003, 2009; Burgers et al., 1998), such as the EFAS system. The EnKF is applied to update state variables of the hydrological model. The forward model is given by:

$$\Psi(t+1) = f(\Psi(t), F(t), p) \tag{2}$$

where f is the set of model equations, i.e. the model structure, representing the hydrological processes that lead to change in the system state over time, $\Psi(t)$ is the state of the model at time t, $F(t)$ the model forcing at time t (e.g. precipitation and evaporation) and p are the model parameters. The EnKF is applied on each daily timestep using observations from remote sensing (AMSR-E, SMOS and ASCAT) and discharge observations. The general form of the EnKF (Evensen, 2003) is given by:

HESSD
10, 13783–13816, 2013

$$\mathbf{\Psi}^{a} = \mathbf{\Psi}^{f} + \mathbf{P}^{f} H^{T} (H P^{f} H^{T} + R)^{-1} (Y - H\mathbf{\Psi}^{f}) \quad (3)$$

where $\mathbf{\Psi}^{a}$ is the analysis of $\mathbf{\Psi}^{f}$, the model forecast, $\mathbf{P}^{f}$ the error covariance matrix of the model, R is the measurement error covariance, H is the measurement operator which relates the model states Ψ to the satellite or discharge observations Y. The observations Y can be described by:

$$Y = H\mathbf{\Psi}^{t} + \epsilon \quad (4)$$

where the true model state ($\mathbf{\Psi}^{t}$) is transformed to the Y, using the measurement operator (H) and random noise ϵ with a zero mean and an error given by the measurement error covariance (R). The state error covariance matrix of the model prediction is directly calculated from the spread between the different ensemble members using:

$$\mathbf{P}^{f} = \overline{(\mathbf{\Psi}^{f} - \mathbf{\Psi}^{t})(\mathbf{\Psi}^{f} - \mathbf{\Psi}^{t})^{T}} \quad (5)$$

where $\mathbf{\Psi}$ is the model state vector and the superscripts f and t represent the forecast and true state, respectively. Since the true state is not known it is assumed that:

$$\mathbf{P}^{f} \approx \mathbf{P}^{f}_{e} = \overline{(\mathbf{\Psi}^{f} - \overline{\mathbf{\Psi}^{f}})(\mathbf{\Psi}^{f} - \overline{\mathbf{\Psi}^{f}})^{T}} \quad (6)$$

where $\overline{\mathbf{\Psi}^{f}}$ represents the ensemble average and it is assumed that the ensemble of model simulations is sufficient to represent the true state. The EnKF is implemented in the PCRaster modelling environment (Karssenberg et al., 2010).

For the assimilation of the satellite data with the Ensemble Kalman Filter (EnKF), spatial information on the measurements error covariance (R, Eqs. 3 and 4) is required. The structure of R is determined from estimates of Wanders et al. (2012, 2013) over Spain obtained using high resolution modelling of the unsaturated zone. From this study the relative errors of each satellite product were determined as well as the spatial

HESSD
10, 13783–13816, 2013

correlation of the errors of the satellites. To avoid errors produced by downscaling of the satellite soil moisture, the average modelled soil moisture at the satellite resolution is directly compared with the satellite soil moisture. The error covariance between the discharge observations is set to zero while the standard error for the discharge observations is assumed to be 0.3 times the discharge, based on expert knowledge. It is assumed that the covariance between the satellite observations and discharge observations equals zero.

2.5 Assimilation and ensemble hindcasting

In this study, observed satellite and discharge data for December 2010–November 2011 are used in a hindcasting experiment for the Upper Danube. Only one year was selected to test the procedure since all satellite products are available for this time period with sufficient data quality. A data assimilation procedure is used to create a reanalysis timeseries of all state variables which are used as starting point for the hindcast (t_0). The 300 parameter realizations from the probabilistic calibration are used to generate the reanalysis timeseries. As meteorological forcing for the reanalysis, observed timeseries of daily precipitation, daily potential evapotranspiration and the average daily temperature is used. Observations are interpolated between meteorological stations with an inverse distance interpolation. For every timestep up till t_0, observed state variables, remotely sensed soil moisture and/or discharge (depending on the scenario), are assimilated into the model. However, parameters are not updated and remain constant for the complete reanalysis timeseries.

At t_0, the start of the hindcast, the forward model (Eq. 2) is used for the hindcasting of discharge and other state variables. After t_0, the daily forcing from the ECMWF-EPS is used to drive the model simulation. The hindcast is evaluated based on the observed discharge for the hindcasting period. Like in EFAS hindcasts are done at midday and midnight based on the latest simulations of the ECMWF-EPS leading to a total of 730 hindcasts. In the original forecasts from EFAS only one set of inital conditions is used, thereby neglecting the uncertainty in the initial conditions. In this experiment, 300

HESSD
10, 13783–13816, 2013

possible realizations of the initial conditions are available from the reanalysis. For each hindcast the 51 members of the ECMWF-EPS are used twice with random realizations from the 300 members of the reanalysis to create $n = 102$ realizations per hindcast. In this approach different meteorological forcing and initial conditions are used for each hindcast to have a better estimate of the forecast uncertainty. A four month simulation was performed using all 300 members in combination with all 51 meteorological forecasts. An analysis on the probability density functions of each hindcast showed that a total of 102 realizations showed no significant differences with the simulation of 15300 realizations. Hence, to reduce calculation times 102 realizations per hindcast were used in all scenarios which could sufficiently explain the variation in the hindcast. Calculation times for this new assimilation system are low. For a forecast with 102 members for the Upper Danube the required calculation time is 120 s on a 8-core machine with 2.26 GHz processors and 24 GB RAM.

2.6 Scenarios

The different scenarios are given in Table 1 as well as the data used in the assimilation before the hindcasting is done. The parametrization as calibrated by Wanders et al. (2013) was used to create reanalysis time series for each scenario. Moreover, the calibration was based on the observations available for the reanalysis, so if both discharge and satellite data are available these were also used for the calibration of the hydrological model (Table 1).

2.7 Evaluation

The evaluation of each hindcast is done based on coefficient of variation (cv), Continuous Ranked Probability Score (CRPS, Hersbach, 2000), Mean Absolute Error (MAE), Brier Score (BS, Brier, 1950) and the number of false and true positive flood alerts. Theses score are calculated for each lead time separately to evaluate the quality of the hindcast for different lead times.

HESSD
10, 13783–13816, 2013

To asses the spread of the ensemble of simulated discharges, the coefficient of variation is determined with:

$$\mathrm{cv} = \frac{1}{T}\sum_{t=1}^{T}\frac{\sigma_{Q_{\mathrm{mod}}(t)}}{\overline{Q_{\mathrm{mod}}(t)}} \tag{7}$$

where $\sigma_{Q_{\mathrm{mod}}(t)}$ and $\overline{Q_{\mathrm{mod}}(t)}$ ($\mathrm{m}^3\,\mathrm{d}^{-1}$) are the standard deviation and the mean of the ensemble of modelled discharge at time t, respectively, and T is the number of timestep (days) in the reanalysis period.

The CRPS (Hersbach, 2000) is used to calculated whether the uncertainty of the forecast is correct and not over or underestimated. The CRPS is given by:

$$\mathrm{CRPS} = \frac{1}{T}\sum_{i=1}^{T}\int_{x=-\infty}^{x=\infty}(F_i^{\mathrm{f}}(x,t) - F_i^{\mathrm{o}}(x,t))^2\mathrm{d}x \tag{8}$$

where $F_i^{\mathrm{f}}(x,t)$ is the cumulative density function of the hindcast at time t, $F_i^{\mathrm{o}}(x,t)$ is the cumulative density function of the observation at time t. $F_i^{\mathrm{o}}(x)$ is given by a Heaviside function, with a step from 0 to 1 probability at the observed value. The CRPS is standardized by $\overline{Q_{\mathrm{obs}}}$ for each validation location to enable a comparison between stations with a different magnitude of discharge.

To calculate if the hindcasts are biased the MAE is calculated using the ensemble mean of the forecast. The MAE is given by:

$$\mathrm{MAE} = \frac{1}{T}\sum_{t=1}^{T}\frac{|\overline{Q_{\mathrm{mod}}(t)} - Q_{\mathrm{obs}}(t)|}{\overline{Q_{\mathrm{obs}}}} \tag{9}$$

where $\overline{Q_{\mathrm{mod}}(t)}$ and $Q_{\mathrm{obs}}(t)$ ($\mathrm{m}^3\,\mathrm{d}^{-1}$) are the average hindcasted discharge and observed discharge at time t respectively and $\overline{Q_{\mathrm{obs}}}$ is the average discharge over the

HESSD
10, 13783–13816, 2013

evaluation period. cv, CRPS and MAE are used to evaluate the performance of each scenario and to determine the quality of each hindcasting scenario. In addition these scores are determined per lead time separately to enable a better comparison between the different scenarios and also to determine the flood forecasting performance of EFAS for different lead times.

To test the accuracy of the flood alerts (both timing and height of the flood peak), the Brier score is calculated for different flood thresholds and different lead times. The Brier score is calculated by:

$$\mathrm{BS} = \frac{1}{T}\sum_{t=1}^{T}(f(t) - o(t)) \tag{10}$$

where $f(t)$ is the probability that discharge will exceed a certain threshold (calculated from the probability density function) and $o(t)$ is a binary value which is 0 if this threshold is not exceeded and 1 if it is exceeded. The Brier score can be calculated for different thresholds of discharge and different lead times. In this study we focus on two threshold levels namely the 80th and 90th percentile of the discharge (Q_{80}, Q_{90}). Exceedance of these arbitrary levels will not necessarily cause flood situation, however to allow for evaluation of hindcast these high discharge events are used. Furthermore the number of false positives (flood forecast, no flood observed), missed (no flood forecasted, flood observed) and correctly forecasted (flood forecasted, flood observed) were calculated for each hindcasting scenario for the Q_{80} and Q_{90}.

3 Results

3.1 Reanalysis

To analyse the performance of the reanalysis the cv (Eq. 7) is used to determine the uncertainty after the assimilation of the observations (Fig. 3 and Table 2). In the $Q0$

HESSD
10, 13783–13816, 2013

scenario, the model is not calibrated and no data is assimilated into the reanalysis to correct for incorrect model states. The uncertainty in the model simulation is large with a cv of 0.25. Uncertainty is even increased in extreme flood events, reducing the potential to use a model calibrated on expert knowledge without data assimilation for flood forecasting. The assimilation of three different satellite products ($Q0_{sat}$) results in a reduction of the cv of the discharge simulation to 0.136 compared to 0.25 for $Q0$ (Fig. 3). This reduction is caused by the reduction in uncertainty of the simulated soil moisture content (not shown), due to the assimilation of the soil moisture observations. However, soil moisture observations can not be used to calibrate groundwater and routing parameters, since they do not contain information on groundwater and routing processes. This results in the fact that the discharge simulations are not necessarily improved (also found by Wanders et al., 2013). Two scenarios are created where discharge is assimilated into the model, namely $Q1$ and $Q7$. For $Q1$ only discharge from the outlet has been used and for $Q7$, additional discharge observations (Fig. 1) upstream are assimilated into the model. The assimilation of additional observation data reduces the cv of 0.08 for $Q1$ to 0.04 for $Q7$, which is for both scenarios lower than for $Q0$ (Table 2). Finally, two scenarios where both discharge and remotely sensed soil moisture observations are assimilated into the model ($Q1_{sat}$ and $Q7_{sat}$) are used to create a reanalysis timeseries. In these scenarios the uncertainty is reduced compared to most other scenarios. However, peak discharge for $Q1_{sat}$ are overestimated, while baseflow simulations are better compared to $Q1$. Improved simulations are also observed to $Q7_{sat}$ compared to $Q7$ and the problem with overestimated peak discharge is none existing for $Q7_{sat}$ (Fig. 3). It must be mentioned that additional discharge data has a larger impact on the reduction of the uncertainty, than assimilation of remotely sensed soil moisture. However, remotely sensed soil moisture enables a better simulation of the base flow compared to assimilation of discharge observation only. The reduction in uncertainty with the assimilation of remotely sensed soil moisture shows that this the method has a high potential in sparsely gauged river basins to correctly simulate discharges across the globe.

HESSD
10, 13783–13816, 2013

3.2 Hindcasting performance

The hindcast performance of each scenario was evaluated using the CRPS (Eq. 8) and the MAE (Eq. 9). In general the uncertainty in the hindcast is reduced when more data is assimilated into the system leading to a better hindcast simulation (Fig. 4). When more discharge data is assimilated, the uncertainty is more strongly reduced than with the assimilation of only remotely sensed soil moisture data (Figs. 3 and 4). This is also confirmed by the CRPS score for the different scenarios (Fig. 5), where the decrease in CRPS is strongest when more discharge data is used (Table 2). In general the CRPS increases with increasing lead times for all scenarios with the exception of $Q1_{sat}$. Due to the larger spread for longer lead times (Fig. 4) the CRPS will increase, because forecasts with high uncertainty are penalized. The CRPS for $Q1_{sat}$ is the highest indicating that this scenario has the lowest hindcasting skill of all scenarios (Fig. 5 and Table 2). This is caused by the overestimation of most flood events, which results in a high CRPS. When more discharge data is assimilated ($Q0$ compared to $Q1$ and $Q7$) the CRPS is reduced throughout the catchment for most locations including the outlet near Bratislava. When a combination of discharge data and satellite data is assimilated ($Q7_{sat}$), the quality of the hindcast is highest (Fig. 4).

The MAE (Eq. 9) is calculated for all scenarios for different lead times and locations (Fig. 6). Compared to the scenario without assimilation of observations ($Q0$), only the scenarios where multiple discharge stations are assimilation ($Q7$ and $Q7_{sat}$) show an increase in performance. The best performance is generated by $Q7_{sat}$, which shows a low bias compared to the observed discharge. For $Q1_{sat}$ the MAE is relatively low, especially when compared to the CRPS. This is mainly caused by the accurate discharge simulation in base flow periods, resulting in a low MAE.

3.3 Flood hindcasting skill

The performance of each scenario was evaluated using the BS (Eq. 10) and the number of false positive flood alerts. Due to the high spread within the ensemble the $Q0$

HESSD
10, 13783–13816, 2013

in general has a low forecasting skill (Table 2). This is shown by the relative high BS (Fig. 7) and the high number of false positive forecasts (Fig. 8). Almost all flood events are correctly captured also for long lead times, which is caused by the overestimation of discharge in general (Fig. 4). The overestimation of discharge also causes the high number of false positive flood forecasts, where around 90 % of the exceedances of the threshold are incorrect and no flooding occurs. Compared to $Q0$ the forecasting skill for $Q0_{sat}$ is decreased, shown by an increasing BS and a higher number of false positives. The high number of false positives is the result of an even higher over estimation of the peak discharge in this scenario (Fig. 4), which results in false flood alerts. The number of missed and correctly forecasted floods remains the same. The BS and the number of false postives for $Q1$ and $Q7$ is considerably lower than for $Q0$. $Q7$ also has a better hindcast skill than the $Q1$ caused by the increased number of observations used in the assimilation framework. The improved forecasting skill is also found in the BS for both $Q1_{sat}$ and $Q7_{sat}$ (Fig. 7), which are for both scenarios lower than without the assimilation of remotely sensed soil moisture. The number of false positive flood forecasts is reduced by 70 % compared to the scenarios with only discharge assimilation, while the number of missed and correctly forecasted floods remains the same. This leads to the conclusion that even when the simulation of discharge throughout the catchment is used and discharge simulations are of a high quality, adding satellite data will lead to an improvement in the forecasting skills of the hydrological model.

4 Conclusions

In this study the added value of remotely sensed soil moisture for flood forecasting has been studied in an operational flood forecasting system. The gain from assimilation of soil moisture observations is compared to assimilation of only discharge and the combination of discharge and soil moisture observations. The European Flood Awareness System (EFAS) was used for a hindcasting experiment in the Upper Danube. Hindcasts

HESSD
10, 13783–13816, 2013

have been made for a period of one year and the results have been compared for six different scenarios.

The assimilation of remotely sensed soil moisture has an impact on the simulation of discharge as shown by other studies (e.g. Pauwels et al., 2001; Brocca et al., 2010, 2012; Draper et al., 2011). However, in this study we show that the impact is not only limited to small catchments with a spatial extent close to or smaller than the satellite resolution but also works for larger catchments.

We show that the assimilation of remotely sensed soil moisture improves the flood forecasting especially when used in combination with assimilation of discharge observations. The uncertainty in the discharge simulations are reduced and biases in the simulation are reduced when satellite data is assimilated. In scenarios where only a limited number of observations is used, however, the peak discharges are generally overestimated.

Floods are better predicted when soil moisture data is assimilated into EFAS and the number of false alerts is reduced compared to scenarios when these data are not used. Although the gain of using more discharge observations remains larger, soil moisture observations improve the quality of the flood alerts, both in terms of timing and in the exact height of the flood peak.

In this study the hydrological model has been calibrated using the same observations as used for the assimilation into EFAS. This will ensure that the parametrization of the model is optimal for the correct simulation of the hydrological variables used in the assimilation framework. Most studies only use streamflow observations for the calibration of hydrological models. However, assimilation of remotely sensed soil moisture can lead to significant difference in the parametrization of the hydrological model (e.g. Santanello et al., 2007; Sutanudjaja et al., 2013; Wanders et al., 2013) and this will also impact the potential gain from the assimilation of observations of other hydrological variables.

In this study two thresholds have been derived from the observed data and are used to calculate potential flood in the Upper Danube catchment. However, the thresholds

HESSD
10, 13783–13816, 2013

used in this study (Q_{80} and Q_{90}) are arbitrary levels and do not necessarily correlate with alert levels of the local conditions. In the current EFAS system the multiple alert levels are based upon the model simulations from a 20 yr simulation, to identify the 5 and 20 yr return periods of floods (Roo et al., 2011). In this situation an alert will be issued when this modelled threshold is exceeded and it is not derived from the local conditions. Here the threshold is defined based upon real observations, since it is tested whether the data assimilation framework will improve both absolute levels of the discharge simulation and the temporal correlation between simulation and observations.

An additional scenario has been studied, where only calibration of the hydrological model was used and no assimilation of any observation. This scenario was created to study the added value of the assimilation compared to only calibration of the EFAS system. It is found that the CRPS, MAE and BS are all reduced by the assimilation (not shown). Simulations without data assimilation tend to have biases in the simulation and a larger ensemble spread than scenarios with data assimilation, while the reduced uncertainty resulting from assimilation will lead to a increased reliability of flood forecasts. These results show the added value of assimilation of observations into the EFAS system, compared to the current set-up.

In conclusion, we show that the uncertainty in the flood forecasts is reduced when discharge observations and satellite data are assimilated into the EFAS system. The addition of remotely sensed soil moisture will reduce the number of false positive flood alerts and thereby increase the reliability of the flood awareness system. Although the amount of the data available via satellite retrievals still remain a challenge in an operational system, the potential benefits could lead to a significant reduction in the false flood alerts, in particular for reducing the number of unnecessary precautions taken by the responsible governments and increase the confidence and willingness to act upon these warnings.

HESSD
10, 13783–13816, 2013

Acknowledgements. This research was funded by a grant from the user support program Space Research of NWO (contract number NWO GO-AO/30). JRC is acknowledged for being able to work with the Danube model set-up. GRDC and ECMWF are acknowledged for making publicly available their data. Jutta Thielen is acknowledged for her constructive review of the draft article.

References

Alfieri, L., Burek, P., Dutra, E., Krzeminski, B., Muraro, D., Thielen, J., and Pappenberger, F.: GloFAS – global ensemble streamflow forecasting and flood early warning, Hydrol. Earth Syst. Sci., 17, 1161–1175, doi:10.5194/hess-17-1161-2013, 2013. 13785

Bartalis, Z., Kidd, R., and Scipal, K.: Development and implementation of a Discrete Global Grid System for soil moisture retrieval using the MetOp ASCAT scatterometer, in: 1st EPS/MetOp RAO Workshop, ESA SP-618, 15–17 May 2006, Frascati, Italy, 2006. 13790

Bisselink, B., van Meijgaard, E., Dolman, A. J., and De Jeu, R. A. M.: Initializing a regional climate model with satellite-derived soil moisture, J. Geophys. Res., 116, D02121, doi:10.1029/2010JD014534, 2011. 13790

Bogner, K. A. and Pappenberger, F. B.: Multiscale error analysis, correction, and predictive uncertainty estimation in a flood forecasting system, Water Resour. Res., 47, W07524, doi:10.1029/2010WR009137, 2011. 13785

Bolten, J., Crow, W., Zhan, X., Jackson, T., and Reynolds, C.: Evaluating the utility of remotely sensed soil moisture retrievals for operational agricultural drought monitoring, IEEE J. Sel. Top. Appl., 3, 57–66, doi:10.1109/JSTARS.2009.2037163, 2010. 13786

Brier, G.: Verification of forecasts expressed in terms of probability, Mon. Weather Rev., 78, 1–3, 1950. 13794

Brocca, L., Melone, F., Moramarco, T., Wagner, W., Naeimi, V., Bartalis, Z., and Hasenauer, S.: Improving runoff prediction through the assimilation of the ASCAT soil moisture product, Hydrol. Earth Syst. Sci., 14, 1881–1893, doi:10.5194/hess-14-1881-2010, 2010. 13786, 13800

Brocca, L., Moramarco, T., Melone, F., Wagner, W., Hasenauer, S., and Hahn, S.: Assimilation of surface- and root-zone ASCAT soil moisture products into rainfall runoff modeling, IEEE T. Geosci. Remote, 50, 2542–2555, doi:10.1109/TGRS.2011.2177468, 2012. 13786, 13800

HESSD

10, 13783–13816, 2013

Burgers, G., Van Leeuwen, P., and Evensen, G.: Analysis scheme in the ensemble Kalman filter, Mon. Weather Rev., 126, 1719–1724, 1998. 13791

Claims Journal: Flood damage in central europe causes ^{22}B in Economic Loss: Aon Benfield: Impact Forecasting – June 2013, Global Catastrophe Recap report, available at: http://www.claimsjournal.com/news/international/2013/07/12/23_2685.htm, last access: 13 November 2013. 13785

Clark, M. P., Rupp, D. E., Woods, R. A., Zheng, X., Ibbitt, R. P., Slater, A. G., Schmidt, J., and Uddstrom, M. J.: Hydrological data assimilation with the ensemble Kalman filter: Use of streamflow observations to update states in a distributed hydrological model, Adv. Water Resour., 31, 1309–1324, doi:10.1016/j.advwatres.2008.06.005, 2008. 13785

Crow, W. T., Miralles, D. G., and Cosh, M. H.: A quasi-global evaluation system for satellite-based surface soil moisture retrievals, IEEE T. Geosci. Remote, 48, 2516–2527, 2010. 13790

De Jeu, R. A. M., Wagner, W., Holmes, T. R. H., Dolman, A. J., Van de Giesen, N. C., and Friesen, J.: Global soil moisture patterns observed by space borne microwave radiometers and scatterometers, Surv. Geophys., 28, 399–420, doi:10.1007/s10712-008-9044-0, 2008. 13789

De Roo, A., Wesseling, C., and Van Deursen, W.: Physically-based river basin modelling within a GIS: the LISFLOOD model, Hydrol. Process., 14, 1981–1992, 2000. 13788

Dorigo, W. A., Scipal, K., Parinussa, R. M., Liu, Y. Y., Wagner, W., de Jeu, R. A. M., and Naeimi, V.: Error characterisation of global active and passive microwave soil moisture datasets, Hydrol. Earth Syst. Sci., 14, 2605–2616, doi:10.5194/hess-14-2605-2010, 2010. 13790

Draper, C., Walker, J. P., Steinle, P., De Jeu, R. A. M., and Holmes, T. R. H.: An evaluation of AMSR-E derived soil moisture over Australia, Remote Sens. Environ., 113, 703–710, 2009. 13789

Draper, C., Mahfouf, J.-F., Calvet, J.-C., Martin, E., and Wagner, W.: Assimilation of ASCAT near-surface soil moisture into the SIM hydrological model over France, Hydrol. Earth Syst. Sci., 15, 3829–3841, doi:10.5194/hess-15-3829-2011, 2011. 13786, 13800

Evensen, G.: Sequential data assimilation with a nonlinear quasi-geostrophic model using Monte Carlo methods to forecast error statistics, J. Geophys. Res.-Oceans, 99, 10143–10162, doi:10.1029/94JC00572, 1994. 13791

Evensen, G.: The Ensemble Kalman Filter: theoretical formulation and practical implementation, Ocean Dynam., 53, 343–367, doi:10.1007/s10236-003-0036-9, 2003. 13791

HESSD
10, 13783–13816, 2013

Evensen, G.: The ensemble Kalman filter for combined state and parameter estimation, IEEE Control Syst., 29, 83–104, doi:10.1109/MCS.2009.932223, 2009. 13791

Hersbach, H.: Decomposition of the continuous ranked probability score for ensemble prediction systems, Weather Forecast., 15, 559–570, doi:10.1175/1520-0434(2000)015<0559:DOTCRP>2.0.CO;2, 2000. 13794, 13795

Karssenberg, D., Schmitz, O., Salamon, P., de Jong, K., and Bierkens, M. F. P.: A software framework for construction of process-based stochastic spatio-temporal models and data assimilation, Environ. Model. Softw., 25, 489–502, doi:10.1016/j.envsoft.2009.10.004, 2010. 13788, 13792

Kerr, Y., Waldteufel, P., Richaume, P., Wigneron, J., Ferrazzoli, P., Mahmoodi, A., Al Bitar, A., Cabot, F., Gruhier, C., Juglea, S., Leroux, D., Mialon, A., and Delwart, S.: The SMOS soil moisture retrieval algorithm, IEEE T. Geosci. Remote, 50, 1384–1403, doi:10.1109/TGRS.2012.2184548, 2012. 13789

Liu, Q., Reichle, R. H., Bindlish, R., Cosh, M. H., Crow, W. T., de Jeu, R., De Lannoy, G. J. M., Huffman, G. J., and Jackson, T. J.: The contributions of precipitation and soil moisture observations to the skill of soil moisture estimates in a land data assimilation system, J. Hydrometeorol., 12, 750–765, doi:10.1175/JHM-D-10-05000.1, 2011. 13786

Loew, A., Holmes, T. R. H., and De Jeu, R. A. M.: The European heat wave 2003: early indicators from multisensoral microwave remote sensing?, J. Geophys. Res., 114, D05103, doi:10.1029/2008JD010533, 2009. 13790

Naeimi, V., Scipal, K., Bartalis, Z., Hasenauer, S., and Wagner, W.: An improved soil moisture retrieval algorithm for ERS and METOP scatterometer observations, IEEE T. Geosci. Remote, 47, 1999–2013, doi:10.1109/TGRS.2008.2011617, 2009. 13790

Nester, T., Komma, J., Viglione, A., and Blöschl, G.: Flood forecast errors and ensemble spread – a case study, Water Resour. Res., 48, W10502, doi:10.1029/2011WR011649, 2012. 13785

Njoku, E., Jackson, T. J., Lakshmi, V., Chan, T., and Nghiem, S.: Soil moisture retrieval from AMSR-E, IEEE T. Geosci. Remote, 41, 215–229, doi:10.1109/TGRS.2002.808243, 2003. 13789

Owe, M., De Jeu, R. A. M., and Holmes, T. R. H.: Multisensor historical climatology of satellite-derived global land surface moisture, J. Geophys. Res., 113, F01002, doi:10.1029/2007JF000769, 2008. 13789

HESSD
10, 13783–13816, 2013

Pauwels, V. R., Hoeben, R., Verhoest, N. E., and Troch, F. P. D.: The importance of the spatial patterns of remotely sensed soil moisture in the improvement of discharge predictions for small-scale basins through data assimilation, J. Hydrol., 251, 88–102, doi:10.1016/S0022-1694(01)00440-1, 2001. 13786, 13800

Rakovec, O., Weerts, A. H., Hazenberg, P., Torfs, P. J. J. F., and Uijlenhoet, R.: State updating of a distributed hydrological model with Ensemble Kalman Filtering: effects of updating frequency and observation network density on forecast accuracy, Hydrol. Earth Syst. Sci., 16, 3435–3449, doi:10.5194/hess-16-3435-2012, 2012. 13785

Roo, A. D., Thielen, J., Salamon, P., Bogner, K., Nobert, S., Cloke, H., Demeritt, D., Younis, J., Kalas, M., Bódis, K., Muraro, D., and Pappenberger, F.: Quality control, validation and user feedback of the European Flood Alert System (EFAS), Int. J. Dig. Earth, 4, 77–90, doi:10.1080/17538947.2010.510302, 2011. 13801

Santanello, J., Peters-Lidard, C. D., Garcia, M. E., Mocko, D. M., Tischler, M. A., Moran, M. S., and Thoma, D.: Using remotely-sensed estimates of soil moisture to infer soil texture and hydraulic properties across a semi-arid watershed, Remote Sens. Environ., 110, 79–97, doi:10.1016/j.rse.2007.02.007, 2007. 13800

Scipal, K., Drusch, M., and Wagner, W.: Assimilation of a ERS scatterometer derived soil moisture index in the ECMWF numerical weather prediction system, Adv. Water Resour., 31, 1101–1112, doi:10.1016/j.advwatres.2008.04.013, 2008. 13786

Sutanudjaja, E., de Jong, S., van Geer, F., and Bierkens, M.: Using ERS spaceborne microwave soil moisture observations to predict groundwater head in space and time, Remote Sens. Environ., 138, 172–188, doi:10.1016/j.rse.2013.07.022, 2013. 13800

Thielen, J., Bartholmes, J., Ramos, M.-H., and de Roo, A.: The European Flood Alert System – Part 1: Concept and development, Hydrol. Earth Syst. Sci., 13, 125–140, doi:10.5194/hess-13-125-2009, 2009. 13785

Van Der Knijff, J. M., Younis, J., and De Roo, A. P. J.: LISFLOOD: a GIS based distributed model for river basin scale water balance and flood simulation, Int. J. Geogr. Inform. Sci., 24, 189–212, doi:10.1080/13658810802549154, 2010. 13788

Vrugt, J., Gupta, H., Nualláin, B., and Bouten, W.: Real-time data assimilation for operational ensemble streamflow forecasting, J. Hydrometeorol., 7, 548–565, 2006. 13785

Wagner, W., Lemoine, G., and Rott, H.: A method for estimating soil moisture from ERS scatterometer and soil data, Remote Sens. Environ., 70, 191–207, doi:10.1016/S0034-4257(99)00036-X, 1999. 13790

HESSD
10, 13783–13816, 2013

Wagner, W., Blöschl, G., Pampaloni, P., Calvet, J. C., Bizzarri, B., Wigneron, J. P., and Kerr, Y.: Operational readiness of microwave remote sensing of soil moisture for hydrologic applications, Nord. Hydrol., 30, 1–20, doi:10.2166/nh.2007.029, 2007. 13789, 13790

Wanders, N., Karssenberg, D., Bierkens, M., Parinussa, R., de Jeu, R., van Dam, J., and de Jong, S.: Observation uncertainty of satellite soil moisture products determined with physically-based modeling, Remote Sens. Environ., 127, 341–356, doi:10.1016/j.rse.2012.09.004, 2012. 13792

Wanders, N., Bierkens, M., de Jong, S., de Roo, A., and Karssenberg, D.: The benefits of using remotly sensed soil moisture in parameter identification of large-scale hydrological models, Water Resour. Res., in review, 2013. 13788, 13792, 13794, 13797, 13800, 13807

Wesseling, C., Karssenberg, D., Burrough, P., and Van Deursen, W.: Integrating dynamic environmental models in GIS: the development of a dynamic modelling language, Trans. GIS, 1, 40–48, doi:10.1111/j.1467-9671.1996.tb00032.x, 1996. 13788

HESSD
10, 13783–13816, 2013

Table 1. Hindcasting scenarios for the EFAS system including abbreviations and assimilated data used tot create a re-analysis timeseries from which hindcasts were initiated. The calibration indicates the data used by Wanders et al. (2013) to calibrate the hydrological model.

	Hindcast		Calibration
Scenario	Number of discharge stations	Satellite data	Data for calibration
$Q0$	0 stations	None	None, expert knowledge
$Q0_{sat}$	0 stations	All satellite data	Satellite data
$Q1$	1 stations	None	1 discharge observation
$Q1_{sat}$	1 stations	All satellite data	1 discharge station &satellite data
$Q7$	7 stations	None	7 discharge stations
$Q7_{sat}$	7 stations	All satellite data	7 discharge stations &satellite data

HESSD
10, 13783–13816, 2013

Table 2. Average skill scores for different hindcast scenarios for the EFAS system. Scores are averaged over different forecasting times and for different locations with discharge observation in the Upper Danube (Fig. 1).

Scenario	cv	CRPS	MAE	BS Q_{90}	BS Q_{80}
$Q0$	0.250	0.361	0.600	0.130	0.257
$Q0_{sat}$	0.136	0.288	0.750	0.220	0.363
$Q1$	0.082	0.272	0.682	0.168	0.314
$Q1_{sat}$	0.074	0.311	0.645	0.084	0.177
$Q7$	0.048	0.261	0.452	0.038	0.166
$Q7_{sat}$	0.044	0.256	0.392	0.029	0.096

HESSD
10, 13783–13816, 2013

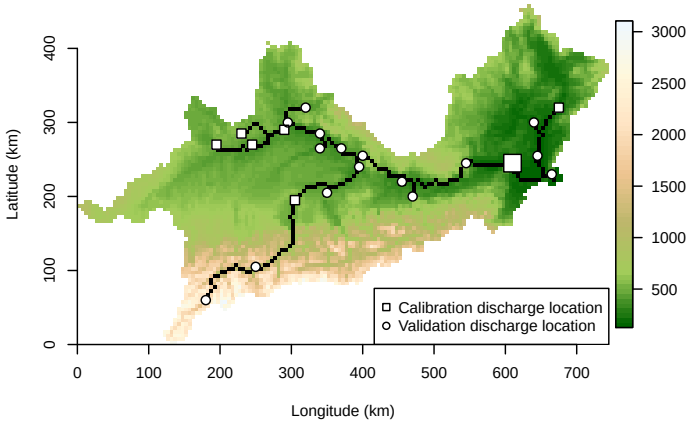

Fig. 1. Digital elevation map of the Upper Danube catchment, colors indicate elevation (m), indicated in black is the river network, square symbols indicate locations for calibration on discharge observations, circles indicate locations for validation on discharge observations. The large square near the outlet (right) is the location used for calibration if only one discharge timeseries is used ($Q1$ and $Q1_{sat}$).

HESSD
10, 13783–13816, 2013

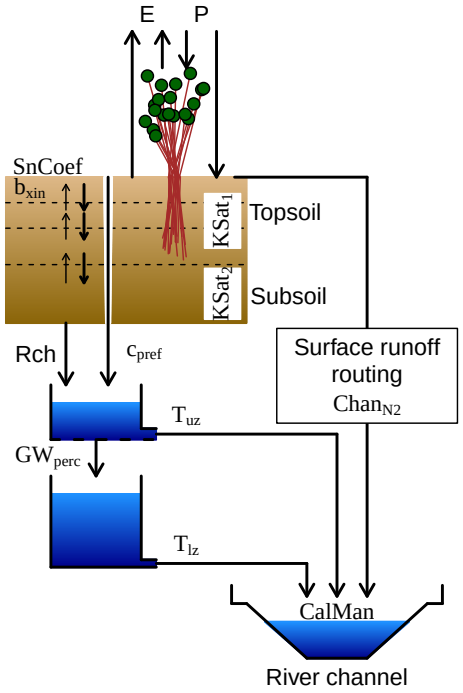

Fig. 2. LISFLOOD model set-up, with fluxes; precipitation (P), evaporation (E), recharge from the unsaturated zone to the groundwater (Rch). The calibration parameters of the model are; snowmelt coefficient (SnCoef), Xinanjiang shape parameter (b_{xin}), saturated conductivity of the topsoil ($KSat_1$), saturated conductivity of the subsoil ($KSat_2$), empirical shape parameter preferential macro-pore flow (c_{pref}), maximum percolation rate from upper to lower groundwater (GW_{prec}), reservoir constant upper groundwater (T_{uz}), reservoir constant lower groundwater (T_{lz}), surface runoff roughness coefficient ($Chan_{N2}$), channel Mannings roughness coefficient (CalMan).

HESSD
10, 13783–13816, 2013

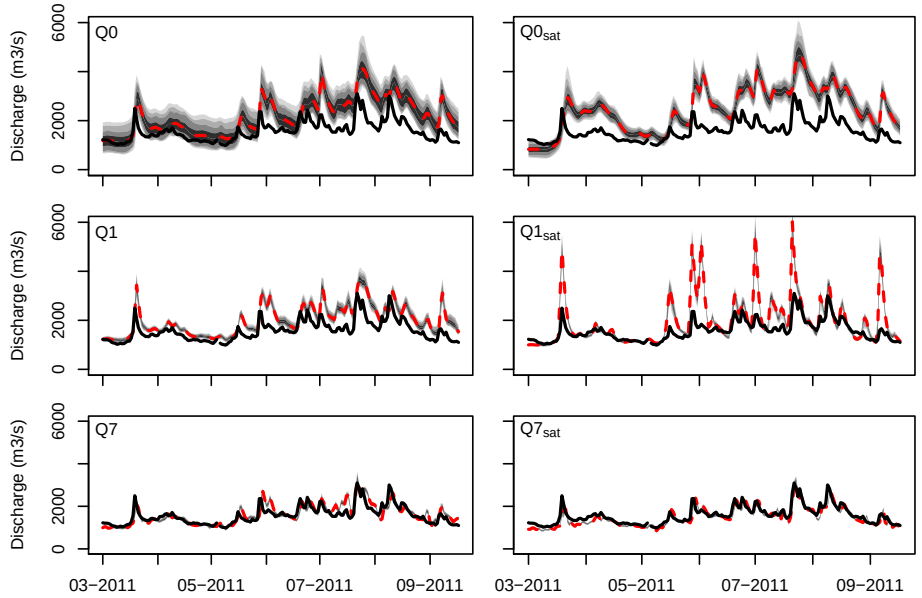

Fig. 3. Reanalysis timeseries of discharge at the outlet of the Upper Danube catchment (Fig. 1) for part of the hindcasting period. In grey are all model realizations, the ensemble mean is given by the red line and the solid black line gives the observed discharge value. The different assimilation scenarios are indicated on the left; for explanation of scenarios see Table 1. Each column of figures gives the hindcast for a particular time, indicated by the vertical line.

HESSD
10, 13783–13816, 2013

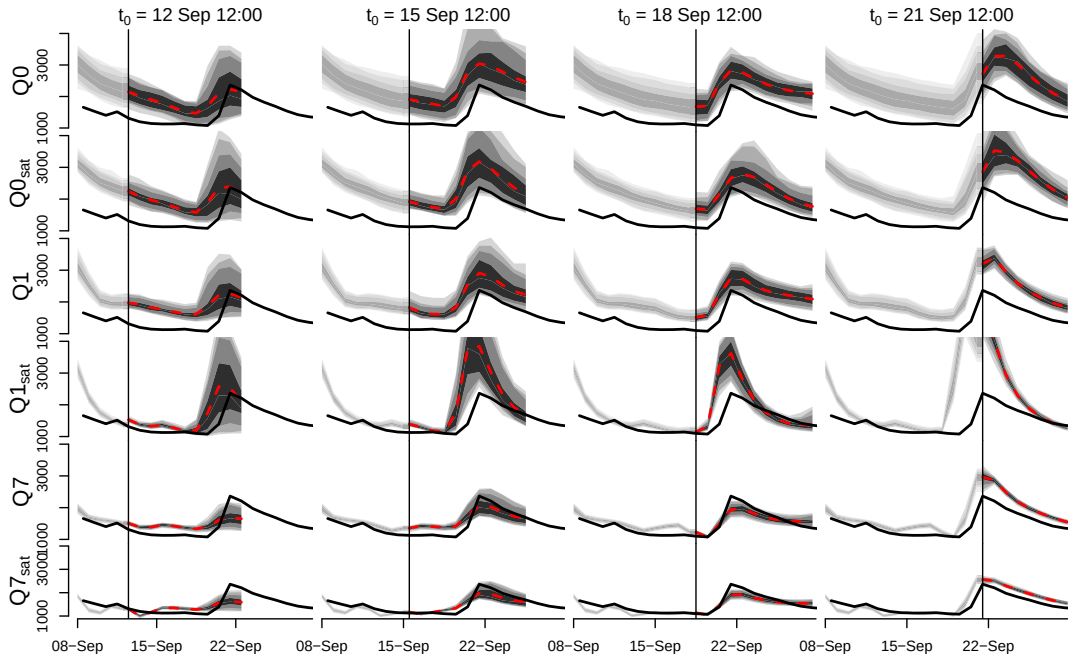

Fig. 4. Example forecast timeseries of discharge at the outlet of the Upper Danube catchment (Fig. 1) for part of the hindcasting period. In grey are all model realizations, the ensemble mean is given by the red dashed line and solid black line gives the observed discharge value. The different assimilation scenarios are indicated in the top left corner of each plot.

HESSD
10, 13783–13816, 2013

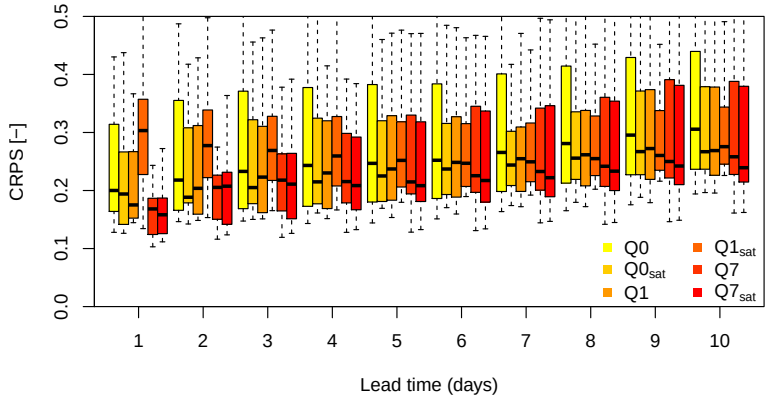

Fig. 5. Continuous Ranked Probability Scores (CRPS) for different forecasting times for the European Awareness Flood System (EFAS). Each boxes contains the CRPS for 16 validation locations for a period of 1 yr with two forecasts per day.

HESSD
10, 13783–13816, 2013

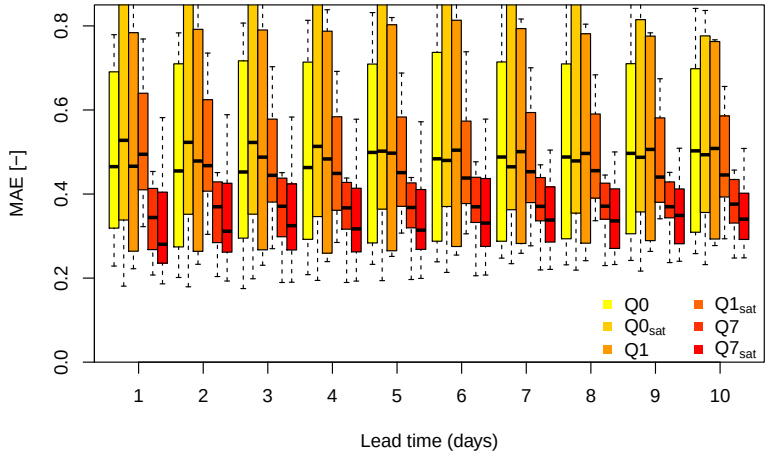

Fig. 6. Mean Absolute Error (MAE) for different forecasting times for the European Awareness Flood System (EFAS). MAE are standardized by dividing the MAE through the mean discharge. Each boxes contains the MAE for 16 validation locations for a period of 1 yr with two forecasts per day.

HESSD
10, 13783–13816, 2013

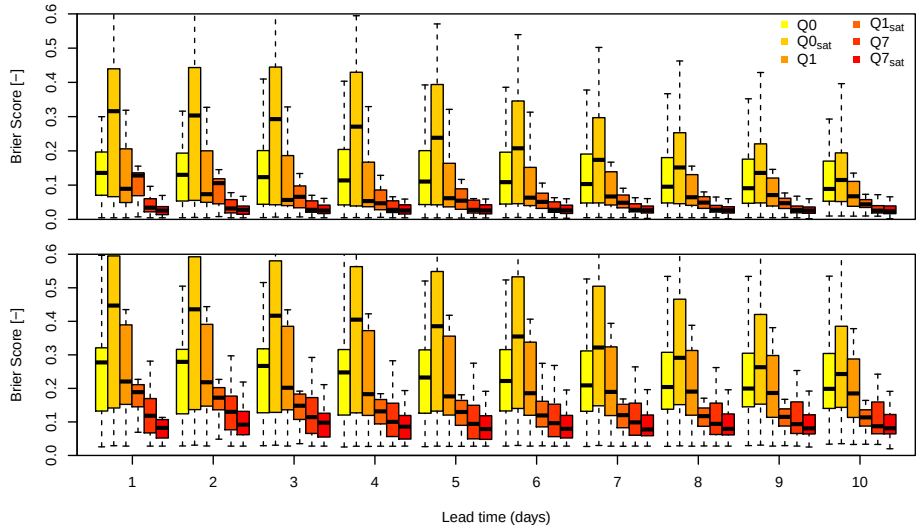

Fig. 7. Brier Score (BS) for different forecasting times for the European Flood Awareness System (EFAS) in the Upper Danube (Fig. 1). Each boxes contains the BS for 16 validation locations for a period of 1 yr with two forecasts per day. The Brier scores for the 90 % threshold (top panel) and the 80 % threshold (bottom panel) are given.

HESSD
10, 13783–13816, 2013

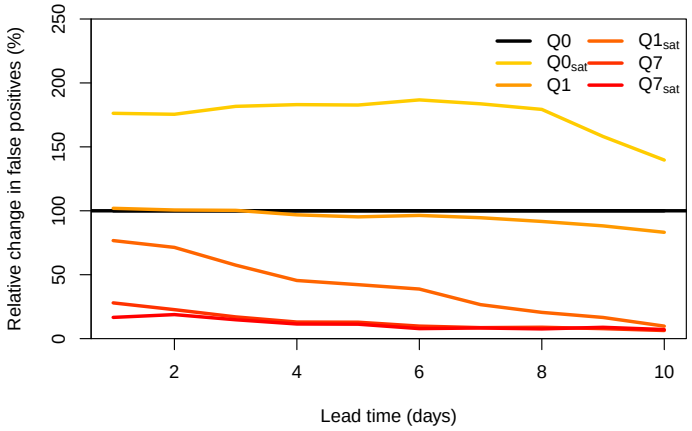

Fig. 8. Relative changes in false positive flood alerts for the 90th percentile threshold, compared to no assimilation scenario (*Q*0) for different forecasting times. A total of 1035 timesteps with flooding were observed for the Upper Danube.

HESSD
10, 13783–13816, 2013